Frontiers in Heat and Mass Transfer (FHMT), 11, 19 (2018)
DOI: 10.5098/hmt.11.19

Global Digital Central
ISSN: 2151-8629

Frontiers in Heat and Mass Transfer

Available at www.ThermalFluidsCentral.org

SORET AND RADIATION EFFECTS ON AN UNSTEADY FLOW OF A CASSON FLUID THROUGH POROUS VERTICAL CHANNEL WITH EXPANSION AND CONTRACTION

N. Vijaya[a, *], Y. Hari Krishna[a], K. Kalyani[b] and G.V.R. Reddy[a]

[a] *Department of Mathematics, K L E F, Deemed to be University, Vaddeswaram, Guntur, Andhra Pradesh-522502,India.*
[b] *Department of Mathematics, VIGNAN'S, Foundation for Science, Technology & Research, Deemed to be University, Vadlamudi, Guntur, Andhra Pradesh-522,India.*

ABSTRACT

The present paper deals with the thermo physical properties of a Casson fluid through an oscillating vertical wall embedded through porous medium under the influence transverse magnetic field, radiation, constant heat source and first order chemical reaction. The radiative heat loss is modelled by using Rosseland approximation. Similarity variables were used to convert the partial differential equations into ordinary differential equation. The transformed ordinary differential equations are solved numerically using Runge - Kutta -Fehlberg method with shooting technique. In order to get perfect perception of the flow pattern we obtain the graphs of axial velocity, temperature and concentrations profiles for various governing parameters viz. Casson parameter, Wall dilation ratio, Reynolds number, Grashoff numbers, Magnetic field parameter, Porous parameter, Radiation parameter, Prandtl number, Heat source parameter, Schmidt's number, Soret number, Chemical reaction parameter. Influence of Skin friction coefficient, Nusselt number, and Sherwood number on both walls are discussed and presented through tabular form.

Keywords: *Casson fluid, Vertical Porous Channel, Soret number, Expanding and contracting Walls, Wall dilation Ratio, Radiation parameter, Schmidt's number.*

1. INTRODUCTION

The study of free and forced convection flow of an in compressible viscous fluid through vertical porous pipes with walls of expansion and contraction under the stature of transverse magnetic field, heat source and radiation has received attention of many researchers due to their extensive range of applications in both technological and biological flows such as transpiration cooling, propellant burning, grain regression, blood flow and artificial dialysis. Especially the flow of a particular fluid in biological organisms is often considered as to be in a porous expanding or contracting vessel. For example, a valve vessel shows deformable boundaries and alternating wall contractions create the effect of a physiological pump. The flow in the lymphatic's also shows a same behavior. Filtration plays a vital role between blood and tissues in many parts of the body. Filtration in biological organisms is often discussed in long circular tubes and extracorporeal duct flows occur between parallel flat membranes.

Uchida and Aoki (1997) examined flow patterns of be of contracting cross section. Ohki (1980) examined the unsteady flow in a semi-infinite tube with porous, elastic wall such that its length varies with time, but its cross section does not vary. Goto and Uchida (1980) investigated the laminar incompressible flow in a semi-infinite porous pipe whose radius varies with time in order to simulate the laminar flow field in cylindrical solid rocket motors. Bujurke et al. (1998) obtained a series solution for unsteady flow in a contracting or expanding pipe. In most of the engineering process like nuclear reactors Geosciences, heat exchanger, coolants and petrology we can observe the physical phenomenon called double diffusion. In coupled free convection heat and mass transfer a mechanisms in clear fluids as well as in porous media, the heat transfer coefficient may increase due to the concentration gradients and a similar increase in mass transfer coefficient due to the thermal gradients. Soret effect (thermo-diffusion) is referred to the mass transfer induced by temperature gradients. Dufour (diffusion-thermo) corresponds to diffusion of heat developed by concentration gradients. In the process of separating isotopes from gases and mixtures from light weight to moderate weight the principle of Soret effect is used. Soret effect is neglected in several studies considering its effect much lower than that of the effect described by Fick's law. However, this effect cannot be neglected as it is found that the flow field in a mixed convective boundary layer over a vertical surface through a porous medium is influenced appreciably by the Soret effect.

Partha (2009) examined the influence of Soret and Dufour on thermophoresis particle deposition in a free convection flow over a semi-infinite vertical surface embedded in a fluid saturated non-Darcy porous medium by maintaining a constant temperature and concentration on the wall in the presence of suction/injection. Vempati et al. (2010) studied the double diffusive effects on the unsteady MHD flow of an electrically conducting, viscous and incompressible fluid over an infinite flat plate under oscillatory suction and thermal radiation. Alao et al. (2015) studied the effect of thermal radiation Soret and Dufour on an unsteady heat and mass transfer flow of a chemically reacting fluid past a semi –infinite vertical plate with viscous

* Corresponding author. Email: vijayanalleboyina@kluniversity.in

Global Digital Central
ISSN: 2151-8629

dissipation. Hari R. Kataria et al. (2016) analyzed the Soret and heat generation effects on MHD Casson fluid past an oscillating vertical plate embedded through porous medium. Subhakar and Gangadhar (2012) investigated the effects of Soret and Dufour on MHD free convection heat and mass transfer flow over a stretching vertical plate with suction and heat source/sink. Olarewaju (2012) studied similarity solution for natural convection from a moving vertical plate with internal heat generation and a convective boundary condition in the presence of thermal radiation and viscous dissipation. In the like manner

Makinde and Mutuku (2014) examined the effect of the complex interaction between the electrical conductivity of the conventional base fluid and that of the nanoparticles under the influence of magnetic field in a boundary layer flow with heat transfer over a convectively heated flat surface using numerical approach called Runge–Kutta–Fehlberg method with shooting technique. Effect of thermal radiation has significant application in physics, space technology and processes operated at very high temperature. For example, in polymer processing industry when the whole system containing the polymer extrusion processes is placed at high temperatures then radiation effect plays a vital role in controlling the heat transfer process. Quality of the end product greatly depends on the rate of heat transfer and hence the knowledge of radiative heat transfer may be helpful to obtain the final product with best quality. Hossain et al. (2001) examined the influence of thermal radiation on free convective flow of an optically thick incompressible viscous fluid over a heated vertical permeable plate by prescribing a constant temperature on the surface. Singh (2008) discussed the effect of radiative heat transfer and heat source on the flow of a viscoelastic fluid over a stretching sheet. Hayat et al. (2012) obtained the Homotopy solutions to explore the impact of thermal radiation and heat source on the Jeffrey fluid flow in a porous medium with power law flux. Study of flows of non-Newtonian fluids has been attracting researchers due to their diverse range of applications both, in nature and technology. Many industrial fluids encountered in chemicals, Cosmetics, pharmaceutics, food and other processing industries such as suspensions, foams, emulsions, colloidal suspensions, polymeric liquids and gels show the non-Newtonian behavior. Casson fluid is one such non-Newtonian fluid used to model fluids like paints, polymer liquids, blood and other industrial fluids.

Sarojamma et al. (2014) examined heat and mass transfer on the MHD boundary layer flow of a chemically reacting non-Newtonian fluid over a stretching sheet with suction. Vijaya. N et al. (2017) studied non liner radiation effect on Casson fluid saturated Non Darcy porous medium. Vijayalakshmi.R et al. (2017) explored the unsteady flow of a Casson fluid through a vertical channel with walls of expansion and contraction. Majdalani et al. (2002) and Dauenhauer et al. (1999) obtained both numerical and asymptotical solution for different Reynolds numbers. Arifizzaman et al. (2018) studied chemically reactive and Naturally Convective High-Speed MHD Fluid Flow through an Oscillatory Vertical Porous-Plate with Heat and Radiation Absorption Effect. Arifizzaman et al. (2017a) examined higher order chemical reactions in micro polar fluids under cross diffusion and MHD effects. Arifizzaman et al. (2017b) investigated MHD Maxwell fluid flow in presence of nano-particle through a vertical porous–plate with heat- generation, radiation absorption and chemical reaction. Arifizzaman et al. (2017c) explored chemically reactive viscoelastic fluid flow in presence of Nano particle through porous stretching sheet. Khan et al. (2012) studied unsteady MHD free convection boundary-layer flow of a Nano fluid along a stretching sheet with thermal radiation and viscous dissipation effects. Biswas et al. (2017) Impacts of magnetic field and radiation absorption on mixed convective Jeffrey Nano fluid flow over a vertical stretching sheet with stability and convergence analysis.

2. MATHEMATICAL FORMULATION

An incompressible unsteady flow of an electrically conducting Casson fluid in a vertical porous channel with contracting and expanding walls under the influence of magnetic field and radiation effect is analyzed. Magnetic field is applied in y-direction externally. Magnetic Reynolds number is very small and can be avoided because of the fact that induced magnetic field is very low compared to the applied Magnetic field. The two walls of the channel are separated by a distance of $2b(t)$, and this distance is smaller than the width and length of the channel. Here both the channel walls are assumed to have the same permeability to contract or expand uniformly at the time dependent rate $\dot{b}(t)$ .The origin is chosen at the middle of the channel. The geometrical interpretation is shown in the Fig. 1.

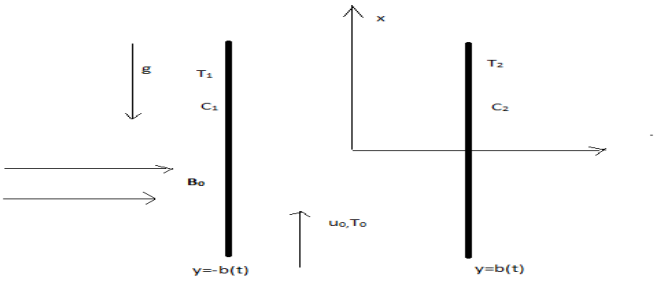

Fig. 1. Geometrical model of the flow

The constitutive equation of the Casson fluid can be written as (Eldabe and Salwa (1995)

$$\tau_{ij}=\begin{cases}2\left(\mu_B+\dfrac{P_y}{\sqrt{2\pi}}\right)e_{ij}, \pi>\pi_c\\ 2\left(\mu_B+\dfrac{P_y}{\sqrt{2\pi_c}}\right)e_{ij}, \pi<\pi_c\end{cases} \tag{1}$$

where τ_{ij} is the $(i,j)^{th}$ stress tensor component. μ_B is the plastic dynamic viscosity of the non-Newtonian fluid, P_y is the yield stress of the fluid, π is the product of the component of deformation rate with itself, namely, $\pi=e_{ij}e_{ij}$, and e_{ij} is the $(i,j)^{th}$ component of deformation rate, and π_c is critical value of π based on non-Newtonian model, Under the Boussineq's approximation, the governing equations for the problem are:

$$\frac{\partial u'}{\partial x}+\frac{\partial \upsilon'}{\partial y}=0 \tag{2}$$

$$\frac{\partial u'}{\partial t}+u'\frac{\partial u'}{\partial x}+\upsilon'\frac{\partial u'}{\partial y}=-\frac{1}{\rho}\frac{\partial P}{\partial x}+\nu\left(1+\frac{1}{\beta}\right)\left(\frac{\partial^2 u'}{\partial x^2}+\frac{\partial^2 u'}{\partial y^2}\right)+ g\beta_T\left(T-T_2\right)+g\beta_C\left(C-C_2\right)-\frac{\sigma B_0^{\,2}}{\rho}u'-\frac{\nu}{k^*}u' \tag{3}$$

$$\frac{\partial \upsilon'}{\partial t}+u'\frac{\partial \upsilon'}{\partial x}+\upsilon'\frac{\partial \upsilon'}{\partial y}=-\frac{1}{\rho}\frac{\partial P}{\partial y}+\nu\left(1+\frac{1}{\beta}\right)\left(\frac{\partial^2 \upsilon'}{\partial x^2}+\frac{\partial^2 \upsilon'}{\partial y^2}\right) \tag{4}$$

$$\rho c_p\left(\frac{\partial T}{\partial t}+u'\frac{\partial T}{\partial x}+\upsilon'\frac{\partial T}{\partial y}\right)=k\left(\frac{\partial^2 T}{\partial x^2}+\frac{\partial^2 T}{\partial y^2}\right)+Q(T-T_2)-\frac{\partial q_r}{\partial y} \tag{5}$$

$$\left(\frac{\partial C}{\partial t}+u'\frac{\partial C}{\partial x}+\upsilon'\frac{\partial C}{\partial y}\right)=D_M\left(\frac{\partial^2 C}{\partial x^2}+\frac{\partial^2 C}{\partial y^2}\right)+D_T\left(\frac{\partial^2 T}{\partial x^2}+\frac{\partial^2 T}{\partial y^2}\right) - k_0\left(C-C_2\right) \tag{6}$$

Here, u' and υ' are the velocity components in the x and y directions respectively, ρ is the density, P is the pressure, ν is the kinematic viscosity, β is the Casson parameter, g is the acceleration due to gravity, β_T is the volumetric coefficient of thermal expansion, T is the

Global Digital Central
ISSN: 2151-8629

temperature, β_C is the coefficient of expansion with concentration, C is the concentration field, σ is the electrical conductivity, B_0 is the strength of the external magnetic field, k^* is the permeability of porous medium c_p is specific heat at constant pressure, k is the thermal conductivity, Q is the heat source parameter, D_M is mass diffusion coefficient, D_T thermal diffusion coefficient, k_0 is the chemical reaction of the fluid.

The boundary conditions for the problem are

$$\begin{aligned} &u'(x,-b)=0, \quad \upsilon'(x,-b)=-\upsilon_W=-B\dot{b}, \\ &T(x,-b)=T_1, \quad C(x,-b)=C_1, \\ &u'(x,b)=0, \quad \upsilon'(x,b)=\upsilon_w=B\dot{b}, \\ &T(x,b)=T_2, \quad C(x,b)=C_2, \end{aligned} \tag{7}$$

The wall permeability is denoted by B and the dots denote the first order derivative with respect to time‘ t’. Here $T_1,T_2,C_1,C_2\left(T_1>T_2\right)$ are the firm temperatures and concentrations of the fluid at both the left and right walls. To apply the radiation effect on the given flow we have considered the application of Rosseland diffusion approximation as reported in the Adegbie and Fagbade (2015) such that

$$q_r=-\frac{4\sigma s}{3k_e}\frac{\partial T^4}{\partial y} \tag{8}$$

Where σs is the Stefan-Boltzman constant and k_e is the mean absorption coefficient. The present study is limited to optically thin fluids so the temperature difference with in the fluid is sufficiently small then Eq. (8) can be linearized by expanding T^4 about T_∞ using Taylor series and neglecting higher order terms we get

$$T^4=4T_\infty^3T-3T_\infty^4 \tag{9}$$

In view of the equations (8) and (9) Eq. (5) reduces to

$$\rho c_p\left(\frac{\partial T}{\partial t}+u'\frac{\partial T}{\partial x}+\upsilon'\frac{\partial T}{\partial y}\right)=k\left(\frac{\partial^2T}{\partial x^2}+\frac{\partial^2T}{\partial y^2}\right)+Q+\frac{16\sigma_ST_\infty^3}{3k_e}\left(\frac{\partial^2T}{\partial y^2}\right) \tag{10}$$

3. METHOD OF SOLUTION

The following similarity transformations are introduced to solve the governing partial differential equation

$$\eta=\frac{y}{b(t)},u'=-\nu b^{-2}xF_\eta(\eta,t),\upsilon'=\nu b^{-1}F(\eta,t),\theta=\frac{T-T_2}{T_1-T_2},\phi=\frac{C-C_2}{C_1-C_2} \tag{11}$$

Eliminating pressure from the governing equations, and using Equation (11) in the resulting equations, we get

$$\begin{aligned} &\left(1+\frac{1}{\beta}\right)F_{\eta\eta\eta\eta}+\alpha\left(3F_{\eta\eta}+\eta F_{\eta\eta\eta}\right)+\left(F_\eta F_{\eta\eta}-FF_{\eta\eta\eta}\right) \\ &-\frac{b^2}{\nu}F_{\eta\eta t}-G_R\theta_\eta-G_C\phi_\eta-\left(M+\frac{1}{K}\right)F_{\eta\eta}=0 \end{aligned} \tag{12}$$

$$(1+R)\theta_{\eta\eta}-\Pr\left(\left(F-\eta\alpha\right)\theta_\eta+\frac{b^2}{\nu}\theta_t\right)+Q^*\theta=0 \tag{13}$$

$$\phi_{\eta\eta}+Sc\left(Sr\theta''-\left(F-\eta\alpha\right)\varphi'-\gamma\varphi-\frac{b^2}{\nu}\theta_t\right)=0 \tag{14}$$

where, $\alpha(t)=\frac{b\dot{b}}{\nu}$ is the dimensionless wall dilation rate, $\alpha(t)>0$ represents wall expansion and $\alpha(t)<0$ corresponds to wall contraction.

$\beta=\frac{\mu_\beta\sqrt{2\pi_c}}{py}$ (Casson parameter)

$\xi=\frac{x}{b}$ (Dimensionless parameter)

$G_R=\frac{g\beta_Tb^3\Delta T}{\nu^2\xi}$ (Thermal Grashoff number)

$G_C=\frac{g\beta_Cb^3\Delta c}{\nu^2\xi}$ (Solutal Grashoff number)

$M=\frac{\sigma B_0^2b^2}{\rho\nu}$ (Magnetic parameter)

$K=\frac{b^2}{k^*}$ (Porosity parameter)

$R=\frac{16\sigma_ST_\infty^3}{3k_ek}$ (Radiation parameter)

$\Pr=\frac{\mu cp}{k}$ (Prandtl number)

$Q^*=\frac{Qb^2}{k}$ (Heat source parameter)

$Sc=\frac{\nu}{D}$ (Schmidt number)

$Sr=\frac{D_T\Delta T}{\nu\Delta C}$ (Soret number)

$\gamma=\frac{k_0b^2}{\nu}$ (Chemical reaction parameter)

The non-dimensional boundary conditions acquire the following form:

$$\begin{aligned} &\eta=-1: \quad F=-\mathrm{Re},F_\eta=0,\theta=1,\phi=1 \\ &\eta=1: \quad F=\mathrm{Re}, \quad F_\eta=0,\theta=0,\phi=0 \end{aligned} \tag{15}$$

Where Re is the permeation Reynolds number defined by $\mathrm{Re}=\frac{Bb\dot{b}}{\nu}=\frac{b\upsilon_w}{\nu}$. For suction Re is positive and for injection, it is negative. This number happens to be a small quantity in many biological applications (Fung and Yih, 1968; Womersley, 1955). A similar solution with respect to time can also be obtained following the same lines described by Uchida and Aoki (1977), Majdalani et al. (2003) and Dauenhauer and majdalani (1999). This can be accomplished by considering the case for which the non-dimensional parameter $\alpha(t)=\frac{b_0\dot{b}_0}{\nu}$, where b_0 and $\dot{b}_0$ denote the initial channel height and expansion rate remains constant and $f=f(\eta),\theta=\theta(\eta)$ and $\phi=\phi(\eta)$ which leads to $f_{\eta\eta t}=\theta_t=\phi_t=0$.

Equations (12) - (14) can be normalized by putting $f=\frac{F}{\mathrm{Re}}$

Then equations (12) – (14) take the form

$$\begin{aligned} &\left(1+\frac{1}{\beta}\right)f_{\eta\eta\eta\eta}+\alpha\left(3f_{\eta\eta}+\eta f_{\eta\eta\eta}\right)+\mathrm{Re}\left(f_\eta f_{\eta\eta}-ff_{\eta\eta\eta}\right)-\lambda\theta_\eta-\zeta\phi_\eta+ \\ &\left(M+\frac{1}{K}\right)f_{\eta\eta}=0 \end{aligned} \tag{16}$$

$$(1+R)\theta_{\eta\eta}-\Pr\left(\mathrm{Re}\,f-\eta\alpha\right)\theta_\eta+Q^*\theta=0 \tag{17}$$

$$\phi_{\eta\eta}+Sc\left(Sr\theta''-\left(\mathrm{Re}\,f-\eta\alpha\right)\varphi'-\gamma\varphi\right)=0 \tag{18}$$

Where $\lambda=\frac{G_R}{\mathrm{Re}}$ is Thermal buoyancy parameter and $\zeta=\frac{G_C}{\mathrm{Re}}$ is solutal buoyancy parameter.

The boundary conditions (15) are reduced to

Global Digital Central
ISSN: 2151-8629

$$\eta = 1: \quad f = -1,\ f_\eta = 0, \theta = 1, \phi = 1 \tag{19}$$

$$\eta = 1: \quad f = 1,\ f_\eta = 0,\ \theta = 0, \phi = 0 \tag{20}$$

The skin friction that arises owing to the viscous drag in the vicinity of the walls is calculated as

$$C_{fx} = \frac{\tau w}{\rho \upsilon w^2} \tag{21}$$

where, $\tau_w = \left(\mu_B + \frac{P_y}{\sqrt{2\pi}}\right)\left(\frac{\partial u}{\partial y}\right)_{y=\pm b}$

$$\left(\mathrm{Re}\right)^{\frac{1}{2}} C_{fx} = \left(1 + \frac{1}{\beta}\right) f''(\pm 1) \tag{22}$$

The rate of heat transfer that arises as a result of heat transfer between the fluid and wall is given by

$$Nu = \frac{q_w}{\frac{k}{b}(T_1 - T_2)} = \theta'(\pm 1) \tag{23}$$

Where $q_w = k\left(\frac{\partial T}{\partial y}\right)_{y=\pm b} = \frac{k}{b}(T_1 - T_2)\theta'(\pm 1)$

The Sherwood number which is result of mass transfer is given by

$$Sh = \frac{m_w}{\frac{D}{b}(C_1 - C_2)} = \phi'(\pm 1) \tag{24}$$

Where $m_w = D\left(\frac{\partial C}{\partial y}\right)_{y=\pm b} = \frac{D}{b}(C_1 - C_2)\phi'(\pm 1)$

The ordinary differential equations (16) – (18) are coupled and highly non-linear. These equations along with the boundary conditions (19) and (20) are solved by applying Runge-Kutta-Fehlberg method with shooting technique to obtained numerical solutions.

4. RESULTS AND DISCUSSION

The objective of the investigation is to explore Soret and radiation effects on an unsteady flow of a Casson fluid through an oscillatory vertical walls embedded through porous medium in the presence of magnetic field, constant heat source and first order chemical reaction. To get a physical insight of the problem the velocity, temperature and species concentration are computationally evaluated and presented through graphs using mathematical software MATLAB.

The behavior of axial velocity for a variation in the wall dilation ratio (α) can be observed from Fig. 2. In case of expanding channel, increasing values of α lead to higher axial velocity in the mid region of the channel while it is less near the walls. This is due to the fact that flow towards the center becomes higher to balance the space occurred due to the expansion of the wall and consequently axial velocity near at the center takes higher values. In case of contracting wall (α <0) with increasing contraction, axial velocity in the vicinity of walls takes higher values as the flow towards the walls become greater which in turn leads to lowering of axial velocity near the center. The influence of the Casson parameter effect on Horizontal and axial velocities can be seen in Fig. 3(a) ,Fig. 3(b) and Fig. 4. It is observed that the Horizontal velocity in expanding channel decreases in the left region with increased values of Casson parameter. In a channel of expansion for increased values of Casson parameter axial velocity decreases near the boundaries while in the mid region it increases where as in contracting channel reverse trend occurs. The influence of Reynolds number on horizontal velocity, axial velocity, temperature and concentration can be seen from Fig. 5(a) to Fig. 7**.** Horizontal velocity is seen to be negative in the half region enclosing the wall $\eta = -1$ whereas it shows an opposite behaviour in the other half region enclosing the wall $\eta = 1$. Further, for increasing values of Re in an expanding channel the horizontal velocity decreases in the region $-1 \le \eta \le 0$ while it increases in $0 \le \eta \le 1$. It can be observed that in the case of expanding channel increasing values of Reynolds number (Re) decrease the axial velocities nominally, near the boundaries while a moderate enhancement is observed in the mid region and the maximum value of velocity occurs exactly at midpoint of the channel. In the case of expanding walls temperature decreases for $-1 \le \eta \le -0.2$ and increases for $-0.2 \le \eta \le 1$. In an expanding channel the solute concentration profiles as in the case of temperature profiles are convex curves for Re = 1 and Re=2 with small values of curvature and as Re increases further the curves become concave.

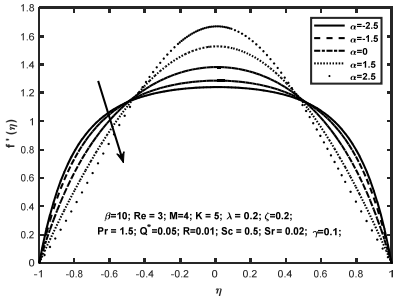

Fig. 2 Axial velocity profiles for various values of α

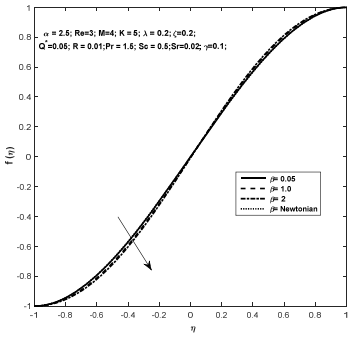

Fig. 3(a) Horizontal velocity profiles for various values of β for $\alpha > 0$

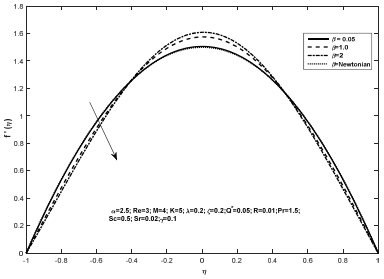

Fig. 3(b) Axial velocity profile for various values of β for $\alpha > 0$

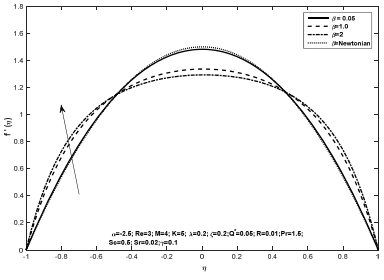

Fig. 4 Axial velocity profile for various values of β for $\alpha < 0$

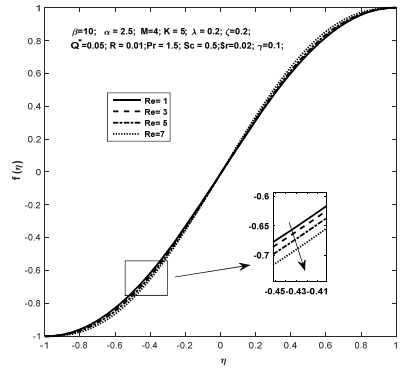

Fig. 5(a) Horizontal velocity profiles for various values of Re for $\alpha > 0$

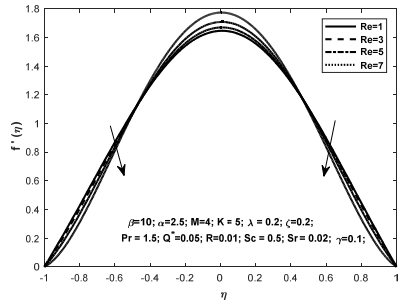

Fig. 5(b) Axial velocity profiles for various values of Re for $\alpha > 0$

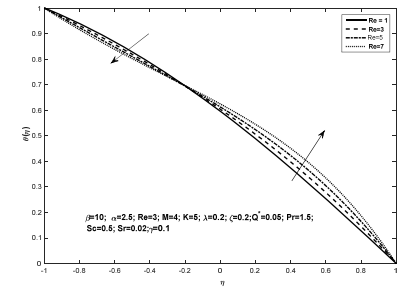

Fig. 6 Temperature profiles for various values of Re for $\alpha > 0$

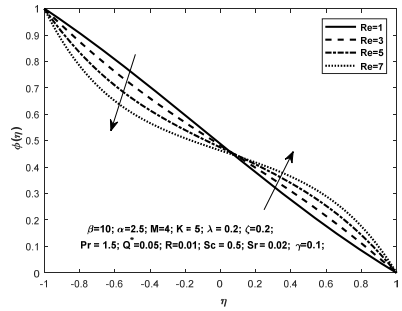

Fig. 7 Concentration profiles for various values of Re for α >0

In an expanding channel, the horizontal velocity is seen to decrease throughout the channel with increasing values of thermal buoyancy parameter λ as shown in Fig.8(a). The axial velocity in both channels diminishes in the left half of the channel with increasing values of thermal buoyancy parameter and attaining a maximum at the midpoint of the channel. As λ increases it is interesting to see that the point of maximum skews towards the wall $\eta = 1$ in an expanding channel. This shows that thermal buoyancy serves as a favorable pressure gradient in the right half region of the expanding channel. This physical phenomenon is observed in Fig. 8(b) and Fig. 9. The influence of solutal buoyancy parameter ζ on velocities is qualitatively similar to that of λ as depicted in Fig. 10(a), Fig.10(b) and Fig. 11. The magnetic parameter M effect on the flow pattern can be seen Fig. 12(a), Fig.12(b) and Fig. 13. In the absence of magnetic field, horizontal velocity profile is concave in the region $-1 \le \eta \le 0$ and is convex in the remaining region. In the presence of magnetic field and with increase in the strength of the magnetic field the concavity of the profiles reduce showing an increase in velocity in the left half of the channel, while a reversal trend is noticed in the right half region. In the absence of M, the axial velocity in an expanding channel increases steadily and gains its maximal value at the mid channel. In the vicinity of magnetic field the velocity increases rapidly for higher values near the boundaries and reduces in the mid region of the channel. For larger strengths of magnetic field, velocity further decreases and the profiles are more blunt in the mid region. In a contracting channel case the velocities show a similar trend in the presence of magnetic field whereas in the absence of magnetic field the velocity rises sharply near the boundaries. The effect of porous parameter K on horizontal and axial velocity is displayed in Fig. 14(a), Fig 4(b) and Fig. 15. For increasing values of K the axial velocity decreases in the region $-1 \le \eta \le 0.4$ and $0.4 \le \eta \le 1$, , and it increases rapidly in the region $-0.4 \le \eta \le 0.4$. The same type of change can be seen for contracting channel however the variation is very small.

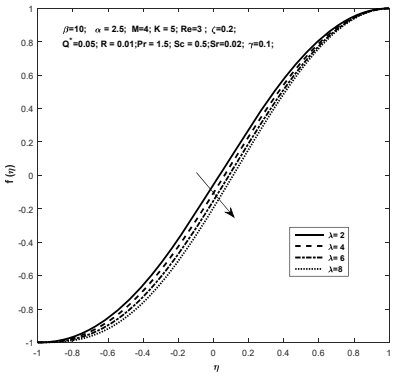

Fig. 8(a) Horizontal velocity profiles for various values of λ for $\alpha > 0$

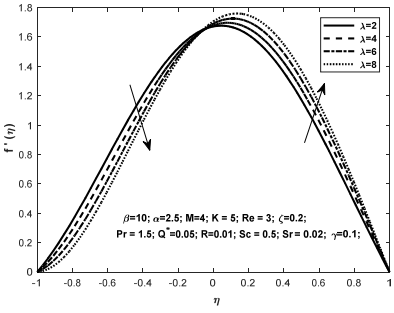

Fig. 8(b) Axial velocity profiles for various values of λ for $\alpha > 0$

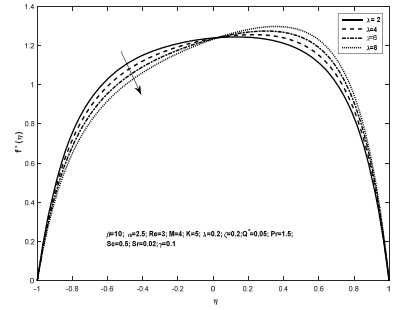

Fig. 9 Axial velocity profiles for various values of λ for α <0

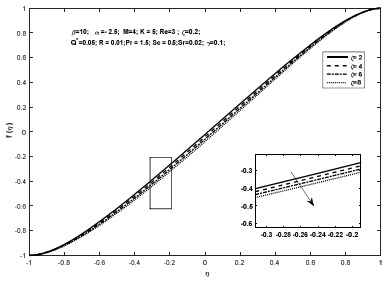

Fig. 10(a) Horizontal velocity profiles for various values of ζ for $\alpha > 0$

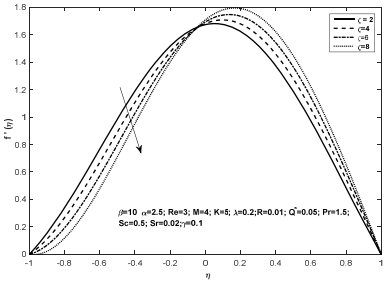

Fig. 10(b) Axial velocity profiles for various values of ζ for $\alpha > 0$

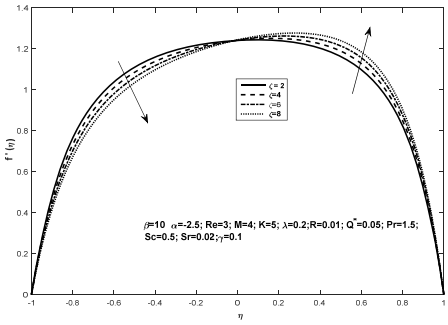

Fig. 11 Axial velocity profiles for various values of ζ for $\alpha < 0$

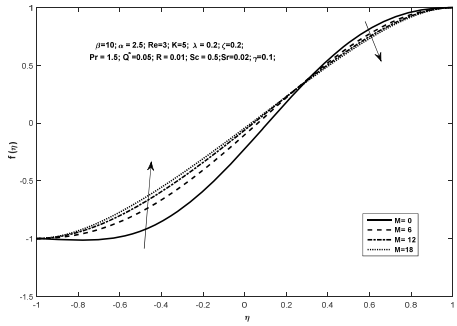

Fig. 12(a) Horizontal velocity profiles for various values of M for $\alpha > 0$

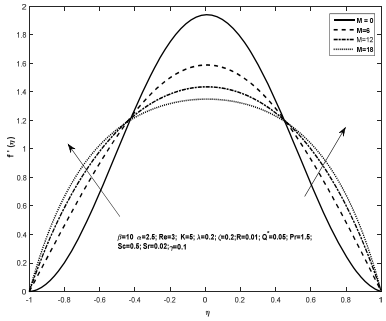

Fig. 12(b) Axial velocity profiles for various values of M for $\alpha > 0$

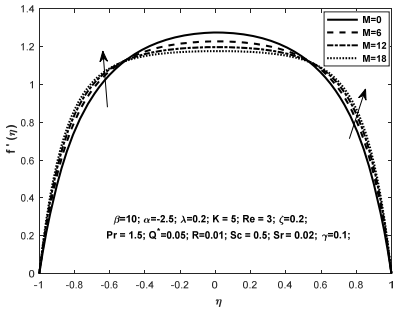

Fig.13 Axial velocity profiles for various values of M for $\alpha < 0$

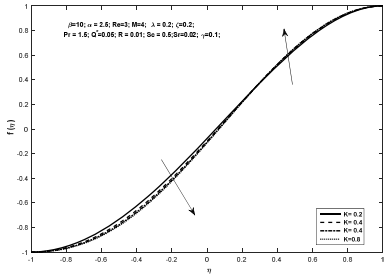

Fig. 14(a) Horizontal velocity profiles for various values of K for $\alpha > 0$

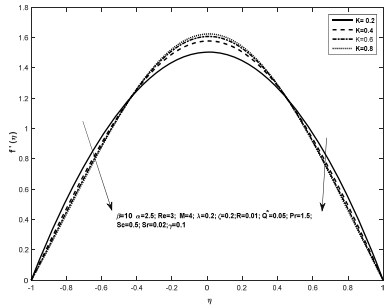

Fig. 14(b) Axial velocity profiles for various values of K for $\alpha > 0$

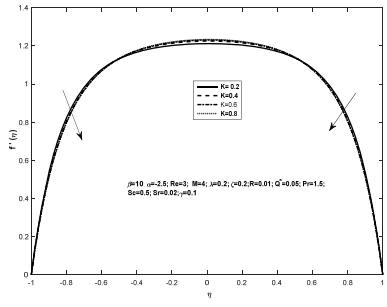

Fig. 15 Axial velocity profiles for various values of K for $\alpha < 0$

The influence of Prandtl number Pr on temperature is seen in Fig. 16 and Fig. 17. In channel of expansion, temperature decreases with increase in Pr in the left region of the channel while it increases in the other half region of the channel. At $\Pr = 0.1$, the temperature is found to be a linear function of η. In a contracting channel an exactly same behavior to that of an expanding channel is observed**.** The heat source parameter Q^* has enhancing influence on temperature throughout the region in the expanding channel which is shown in Fig. 18 and Fig. 19. The effect of thermal radiation R on temperature profile in expanding channel is portrayed in Fig. 20. As radiation increases temperature of the fluid increase in the mid region gradually. From Fig. 21 we observe that as radiation increases the temperature increases rapid near the left boundary and maintain uniform change and decreases rapidly near the

Global Digital Central
ISSN: 2151-8629

boundaries. Fig. 22 and Fig. 23 are the plots of concentration for a variation of Schmidt's number Sc. Concentration in both types of channels is reduced by increasing values of Sc. However, the reduction is rapid near the boundary at $\eta = -1$ in a contracting channel and is almost uniform in the mid region of the channel and the reduction is more significant than that of the expanding channel case. The reduction in species concentration with increasing values of Sc is the result of reducing molecular diffusivity. The effect of Soret number Sr can be seen in Fig. 24 and Fig. 25. As Sr increases the concentration profile increases in the left half of the expanding channel and opposite behavior can be observed in second half of the channel. In the contracting channel the increasing value of Soret number increases concentration. In the region $-1 \le \eta \le 0.8$ and rapidly decreases in the region $0.8 \le \eta \le 1$. The chemical reaction parameter (γ) is found to have a reducing influence on concentration in channels of both types as shown in Fig. 26 and Fig. 27.

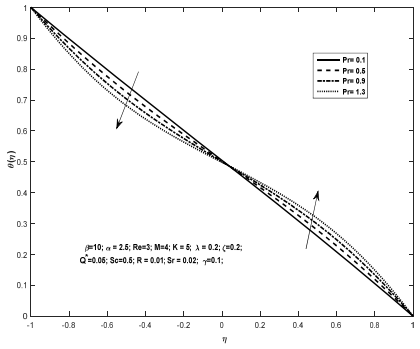

Fig. 16 Temperature profiles for various values of Pr for $\alpha > 0$

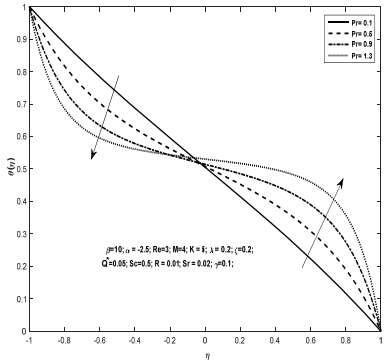

Fig. 17 Temperature profiles for various values of Pr for α < 0

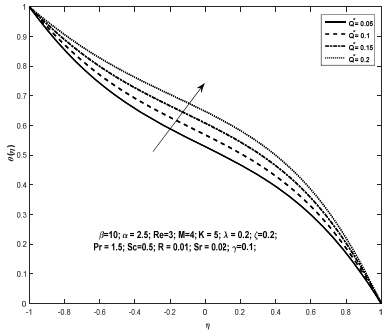

Fig. 18 Temperature profiles for various values of Q^* for $\alpha > 0$

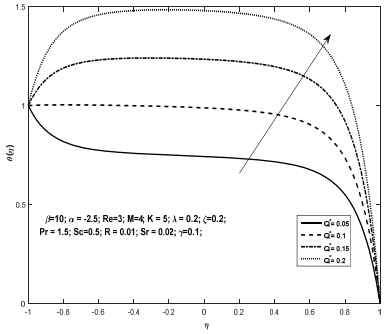

Fig. 19 Temperature profiles for various values of Q* for $\alpha < 0$

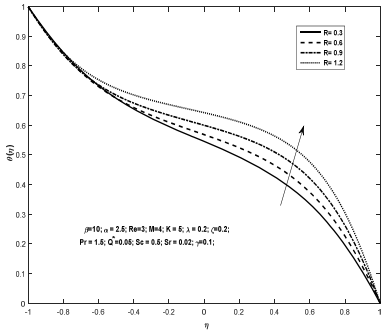

Fig. 20 Temperature profiles for various values of R for $\alpha > 0$

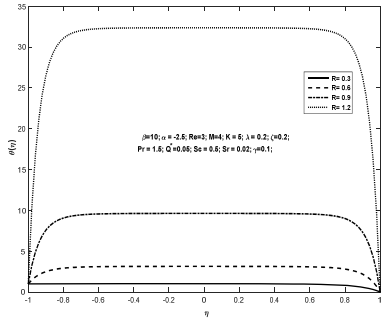

Fig. 21 Temperature profiles for various values of R for $\alpha < 0$

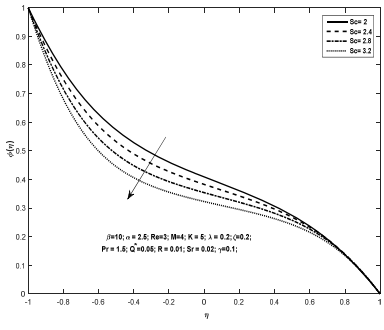

Fig. 22 Concentration profiles for values of Sc for $\alpha > 0$

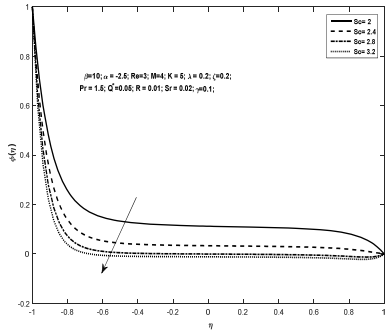

Fig. 23 Concentration profiles for values of Sc for $\alpha < 0$

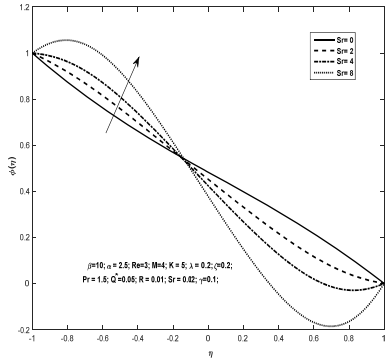

Fig. 24 Concentration profiles for values of Sr for $\alpha > 0$

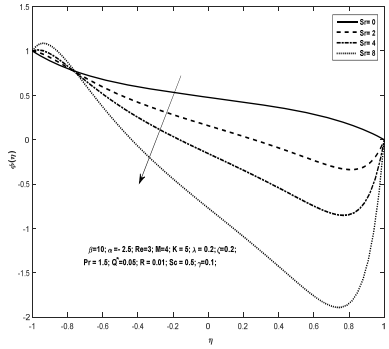

Fig. 25 Concentration profiles for values of Sr for $\alpha < 0$

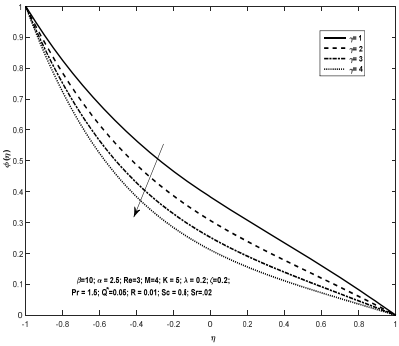

Fig. 26 Concentration profiles for values of γ for $\alpha > 0$

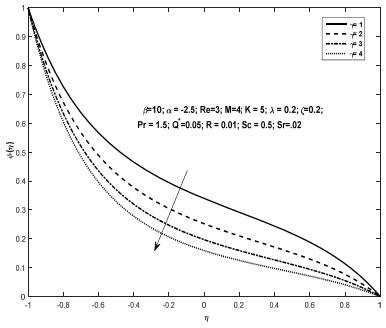

Fig. 27 Concentration profiles for values of γ for $\alpha < 0$

The numerical scheme is validated by comparing the results of the present investigation, that is axial velocity values at different positions of η are compared with those of Majdalani et al. (2002) and Odelu Ojjela et al. (2016) for a Newtonian fluid case $(\beta \to \infty)$ in the absence of $M = \lambda = \zeta = \Pr = Q = Sc = \gamma = 0$. It is observed that there is a fair agreement with Majdalani et al. (2002) and an excellent agreement with Odelu Ojjela et al. (2016). The compared values of axial velocity are presented in Table 1.

Table. 1 The numerical values of axial velocity with present and existing results for $\alpha = 0.5, \mathrm{Re} = 5,\ M = K = \lambda = \Pr = Q^* = R = Sc = Sr = \gamma = 0$ and $\beta \to \infty$

η	Majdalani *et al.* (2002)	Odelu Ojjela *et al.* (2016)	Present
0	1.536002	1.53785	1.53844
0.05	1.531846	1.53344	1.53343
0.1	1.519377	1.52025	1.52026
0.15	1.498596	1.49834	1.49736
0.2	1.469505	1.46782	1.46785
0.25	1.432114	1.42883	1.42788
0.3	1.386445	1.38158	1.38156
0.35	1.332539	1.32627	1.32628
0.4	1.270464	1.26318	1.26312
0.45	1.200325	1.19258	1.19356
0.5	1.122275	1.11478	1.1248
0.55	1.036527	1.03011	1.03111
0.6	0.943364	0.93888	0.937876
0.65	0.843156	0.84142	0.83145
0.7	0.736373	0.73802	0.738077
0.75	0.623597	0.62892	0.62895
0.8	0.505538	0.51432	0.524313
0.85	0.383052	0.39429	0.384278
0.9	0.257149	0.26877	0.268773
0.95	0.129010	0.13751	0.137525
1	0.000000	0.000000	0.000000

The effect of physical parameters Skin friction coefficient, Nusselt number, and Shearwood number is portrayed in Table.2, Table. 3 and Table.4 at both walls at both types of channels.

Global Digital Central
ISSN: 2151-8629

Table 2 Skin friction coefficient for various values of pertinent parameters $\mathrm{Re}=3,\beta=10,\lambda=0.2,\xi=0.2,M=4,K=5,$ $R=0.01,\mathrm{Pr}=1.5,Q^{*}=0.05,Sc=0.5,Sr=0.2,\gamma=0.1$

Variations in pertinent parameters		$\alpha=2.5$		$\alpha=-2.5$	
		$\left(1+\frac{1}{\beta}\right)f''(-1)$	$\left(1+\frac{1}{\beta}\right)f''(1)$	$\left(1+\frac{1}{\beta}\right)f''(-1)$	$\left(1+\frac{1}{\beta}\right)f''(1)$
Re	1	2.1948	-2.3283	-2.3288	-2.3388
	3	1.9424	-2.1264	-2.1264	-2.9264
	5	1.4872	-1.7280	-1.7280	-1.6280
	7	0.6390	-0.8673	0.8673	-0.8673
β	0.05	2.953513	-3.255297	3.148624	-3.467584
	1	2.431667	-2.756879	4.812070	-5.342252
	2	2.189978	-2.527821	5.522042	-6.142252
λ	2	1.546886	-2.491965	7.192858	-7.567086
	4	1.073146	-2.847258	7.084485	-7.766848
	6	0.576983	-3.148314	6.972485	-7.963857
	8	0.070846	-3.399418	6.856871	-8.158039
ζ	2	1.472614	-2.545335	6.976209	-7.677325
	4	0.925741	-2.973187	6.626360	-7.997231
	6	0.359769	-3.360029	6.272263	-8.311879
	8	-0.218304	-3.706481	5.914111	-8.621160
M	0	1.152829	-1.381554	6.955608	-7.062483
	6	1.942487	-2.126405	7.287288	-7.385016
	12	2.572509	-2.727630	7.592869	-7.683490
	18	3.099069	-3.234571	7.877135	-7.962045
K	0.2	3.288311	-3.417642	7.985703	-8.068626
	0.4	2.657121	-2.808831	7.636769	-7.726456
	0.6	2.416353	-2.578044	7.513637	-7.605995
	0.8	2.288804	-2.456134	7.450635	-7.544426
R	0.3	6.636127	-7.389260	1.769143	-2.123979
	0.6	6.660918	-7.411264	1.772520	-2.121789
	0.9	6.729694	-7.483617	1.775936	-2.119999
	1.2	6.937632	-7.710247	1.779426	-2.118691
Pr	0.1	1.7566	1.759258	.761920	11.764578
	0.5	-2.136204	-2.13336	-2.130540	-2.127762
	0.9	6.587577	6.596160	6.604692	6.6122651
	1.3	7.419268	-7.410544	-7.402745	-7.397547
Q*	0.06	1.766139	1.767106	1.768556	1.769522
	0.1	-2.12668	-2.12778	-2.129429	-2.130529
	0.16	6.616691	6.620380	6.625914	6.6296021
	0.2	-7.397352	-7.401429	-7.407543	-7.411617
Sc	2	1.771838	1.773203	1.774406	1.775452
	2.4	-2.114780	-2.11163	-2.108566	-2.105609
	2.8	6.639789	6.641655	6.643450	6.6449821
	3.2	-7.357289	-7.354890	-7.353873	-7.353449
Sr	0	1.763186	1.762759	1.762333	1.761480
	2	-2.130491	-2.13086	-2.131248	-2.132005
	4	6.615829	6.614607	6.613385	6.610941
	8	-7.396286	-7.397227	-7.398169	-7.400053
γ	1	1.763107	1.763026	1.762947	1.762871
	2	-2.130250	-2.129981	-2.129716	-2.129454
	3	6.615682	6.615588	6.615496	6.615407
	4	-7.396114	-7.395873	-7.395636	-7.395402

It is seen that from table 2 that absolute values of Skin friction coefficient at the wall η=-1 decreases with increasing values of Re and K in both types of channels. Higher values of M is found to have increasing influence on absolute values skin friction coefficient in both types of channels .As α changes from negative to positive absolute values the skin friction coefficient at the left wall decreases while it increases at the right wall very small variation can be seen for corresponding changes in remaining parameters.

Table 3 Nusselt number for various values of pertinent parameters $\mathrm{Re}=3,\beta=10,\lambda=0.2,\xi=0.2,M=4,K=5,$ $R=0.01,\mathrm{Pr}=1.5,Q^{*}=0.05,Sc=0.5,Sr=0.2,\gamma=0.1$

Variations in pertinent parameters		$\alpha=2.5$		$\alpha=-2.5$	
		$\theta'(-1)$	$\theta'(1)$	$\theta'(-1)$	$\theta'(1)$
Re	1	-0.2294	-0.2807	-1.7354	-2.5642
	3	-0.7891	-0.9400	-1.8260	-5.5360
	5	-1.6319	-2.4151	3.3574	-13.940
	7	-0.5285	-6.4600	33.1438	-46.848
β	0.05	-0.739438	-0.922788	-1.533398	-5.968484
	1	-0.760177	-0.930880	-1.710076	-5.716067
	2	-0.770478	-0.934241	-1.762154	-5.637021
λ	2	-0.884378	-0.847527	-1.878849	-5.479466
	4	-0.990698	-0.753346	-1.938079	-5.416232
	6	-1.093480	-0.670449	-1.997834	-5.352723
	8	-1.189922	-0.599322	-2.058062	-5.288997
ζ	2	-0.906369	-0.827400	-1.992432	-5.362904
	4	-1.038220	-0.712732	-2.179867	-5.169655
	6	-1.167470	-0.611384	-2.369022	-4.976516
	8	-1.290670	-0.524177	-2.558904	-4.784473
M	0	-0.852056	-0.983202	-1.798220	-5.585673
	6	-0.770550	-0.925005	-1.837523	-5.515505
	12	-0.735768	-0.893033	-1.865006	-5.465563
	18	-0.715487	-0.872226	-1.885277	-5.427800
K	0.2	-0.751561	-0.908181	-1.851481	-5.490288
	0.4	-0.768186	-0.922992	-1.839129	-5.512616
	0.6	-0.774995	-0.928726	-1.834595	-5.520764
	0.8	-0.778705	-0.931766	-1.832240	-5.524986
R	0.3	2.835467	-12.66586	-0.864057	-1.112900
	0.6	26.702216	-39.08965	-0.924215	-1.322932
	0.9	129.13603	-44.04984	-0.954449	-1.574096
	1.2	547.86427	-65.25463	-0.937889	-1.880359
Pr	0.1	-0.469090	-0.572176	-0.545743	-0.668405
	0.5	-0.552329	-0.664932	-1.061846	-1.352088
	0.9	-0.642749	-0.767494	-1.688717	-2.455685
	1.3	-0.739167	-0.879992	-2.035256	-4.206264
Q*	0.06	-0.668405	-0.959686	-1.450056	-5.911806
	0.1	-1.352088	-1.038395	0.053638	-7.414437
	0.16	-2.455685	-1.156441	2.308530	-9.667735
	0.2	-4.206264	-1.23512	3.811360	-11.16950
Sc	2	-0.785681	-0.943617	-1.810886	-5.552040
	2.4	-0.784863	-0.944479	-1.809801	-5.553167
	2.8	-0.784103	-0.945284	-1.809250	-5.553731
	3.2	-0.783403	-0.946028	-1.808891	-5.554091
Sr	0	-0.789104	-0.940043	-1.825851	-1.825851
	2	-0.792613	-0.936560	-1.844051	-1.844051
	4	-0.796124	-0.933079	-1.862344	-1.862344
	8	-0.803153	-0.926122	-1.898882	-1.898882
γ	1	-0.788630	-0.940706	-1.824959	-5.537348
	2	-0.788098	-0.941379	-1.823974	-5.538457
	3	-0.787603	-0.941970	-1.823128	-5.539389
	4	-0.787145	-0.942498	-1.822382	-5.540198

It is noticed from Table 3 that there is considerable enhancement in absolute value of Nusselt numbers for increased values of Re,β ,R ,Pr, Q*,Sc. This is due to the fact that the fluid with low Pr has larger thermal conductivity and this absorbs and converts the temperature gradient at the surface and then leads to surface heat flux. As α moves from positive value to negative value absolute value of Nusselt numbers at the left wall decreases while it increases at the right wall for increased values of λ,K,Sr, γ . Increasing values of M is to enhace absolute value of Nusselt number due to Lorentz force.

Global Digital Central
ISSN: 2151-8629

Table 4 Sherwood number for various values of pertinent parameters $\mathrm{Re}=3, \beta=10, \lambda=0.2, \xi=0.2, M=4, K=5, R=0.01, \mathrm{Pr}=1.5, Q^{*}=0.05, Sc=0.5, Sr=0.2, \gamma=0.1$

Variations in pertinent parameters		$\alpha=2.5$		$\alpha=-2.5$	
		$\phi'(-1)$	$\phi'(1)$	$\phi'(-1)$	$\phi'(1)$
Re	1	-0.434394	-0.391989	-0.924333	-0.819360
	3	-0.648382	-0.575781	-1.269381	-1.071505
	5	-0.941039	-0.807241	-1.757173	-1.285302
	7	-1.351918	-1.069552	-2.661116	-1.171723
β	0.05	-0.633511	-0.571888	-1.300855	-1.091455
	1	-0.639773	-0.573688	-1.283052	-1.080375
	2	-0.642844	-0.574454	-1.277148	-1.076585
λ	2	-0.668977	-0.556128	-1.273882	-1.066746
	4	-0.691851	-0.535462	-1.278933	-1.061454
	6	-0.714108	-0.516438	-1.284032	-1.06158
	8	-0.735329	-0.499224	-1.289179	-1.050862
ζ	2	-0.673710	-0.551777	-1.284846	-1.056645
	4	-0.702049	-0.526237	-1.302080	-1.040302
	6	-0.730223	-0.502130	-1.319364	-1.024137
	8	-0.757909	-0.479608	-1.336692	-1.008153
M	0	-0.668662	-0.585442	-1.275156	-1.073571
	6	-0.642339	-0.572461	-1.267093	-1.070586
	12	-0.630932	-0.565401	-1.261700	-1.068239
	18	-0.624240	-0.560808	-1.257717	-1.066364
K	0.2	-0.636118	-0.568737	-1.264347	-1.069421
	0.4	-0.641568	-0.572016	-1.266775	-1.070455
	0.6	-0.643788	-0.573283	-1.267673	-1.070824
	0.8	-0.644996	-0.573956	-1.268141	-1.071013
R	0.3	-1.310290	-1.043990	-0.648867	-0.576736
	0.6	-1.414814	-0.949137	-0.649167	-0.577387
	0.9	-1.712342	-0.658428	-0.649379	-0.577836
	1.2	-2.604427	0.229239	-0.649559	-0.578143
Pr	0.1	-1.069421	-0.578831	-1.281832	-1.128736
	0.5	-1.070455	-0.578084	-1.274908	-1.120521
	0.9	-1.070824	-0.577240	-1.267787	-1.107664
	1.3	-1.071013	-0.576294	-1.265452	-1.087220
Q*	0.06	-0.648606	-0.575555	-1.274646	-1.066234
	0.1	-0.649503	-0.574651	-1.295704	-1.045152
	0.16	-0.650848	-0.573294	-1.327281	-1.013539
	0.2	-0.651745	-0.572390	-1.348326	-0.992470
Sc	2	-1.264324	-0.770263	-8.961702	-0.849533
	2.4	-1.478726	-0.799343	-11.92464	-0.93904
	2.8	-1.716431	-0.812997	-14.57256	-0.941620
	3.2	-1.977639	-0.821106	-16.98571	-0.957303
Sr	0	-0.651253	-0.580403	-1.279595	-1.133820
	2	-0.360322	-0.122021	-0.235139	5.073601
	4	-0.061657	0.328669	0.856252	11.232167
	8	0.558921	1.207004	3.179579	23.403219
γ	1	-0.945821	-0.422360	-1.807466	-0.687879
	2	-1.207809	-0.310983	-2.202674	-0.453319
	3	-1.425072	-0.235714	-2.494123	-0.312546
	4	-1.612637	-0.182596	-2.727564	-0.221111

It is observed from Table 4 that absolute value of Sherwood number is seen to be an increasing function of Re, K, R, and Sc. For increased values of M there is absolute reduction in Sherwood number. This number has opposite behavior in both types of channels for higher values of λ, ξ .It is seen to diminish with increasing values of M due to the Lorentz force.

5. CONCLUSIONS

Numerical solutions are obtained for the flow of a Casson fluid in a vertical expanding and contracting channel with permeable walls. The velocities in the horizontal and vertical directions, temperature and species concentrations are computationally evaluated. To get a physical insight into the physics of the problem these flow characteristics are graphically presented and discussed for the various parameters governing the flow. Some of the important conclusions are listed below:

- In the case of expanding walls $(\alpha>0)$, increasing values of wall expansion ratio lead to higher axial velocity at in the mid region of the channel and lower velocity near the walls.
- In a contracting channel, $(\alpha<0)$ increasing $|\alpha|$ tends to lower axial velocity near the center while a reverse trend in the vicinity of walls.
- For increasing values of the Casson parameter the axial velocity at the centre of the channel increases while it reduces near the walls of the channel.
- Increase in magnetic parameter tends to enhance the axial velocity near the walls while a reverse effect in the mid region is observed in both channels.
- In both types of channels, temperature and concentration decrease in the left half of the channel while it increases in the other half for increasing values of Re.
- Increasing value of porous parameter (K) decreases axial velocity in both type of channels near the walls and increases in mid region.
- Radiation parameter (R) increases temperature in both type of channels.
- Increasing value of Soret (Sr) parameter increases concentration profiles in the left half of the channel and decreases in right half of the channel.
- Increasing values of porosity parameter decreases axial velocity profiles near the walls and rapidly increases at the centre.

REFERENCES

Adegbie, KS., Fagbade, A.I., 2015, "Influence of variable fluid properties and radiative heat loss on Magnetohydrodynamic forced convection flow in a fluid saturated porous medium," *J Niger Assoc Math Phys,* **30**, 101–116.

Alao, A.I., Fagbade, Falodun, 2016, "Effects of thermal radiation, Soret and Dufour on an unsteady heat and mass transfer flow of a chemically reacting fluid past a semi-infinite vertical plate with viscous dissipation," *Journal of Nigerian Mathematical Society* **35,**142-158. https://doi.org/10.1016/j.jnnms.2016.01.002

Arifuzzaman, S. M., Khan,M.S., Mehedi, Rana and Ahmmed., 2018, "Chemically Reactive and Naturally Convective High-Speed MHD Fluid Flow through an Oscillatory Vertical Porous-Plate with Heat and Radiation Absorption Effect, Engineering Science and Technology,' *an International Journal*, **21**(2), 215-228. https://doi.org/10.1016/j.jestch.2018.03.004.

Arifuzzaman, S. M., Rana, B. M. J., Ahmed,R., and Ahmmed, S. F., 2017a, "Cross Diffusion and MHD effect on a High Order Chemically Reactive Micropolar Fluid of Naturally Convective Heat and Mass Transfer past through an Infinite Vertical Porous medium with a Constant Heat Sink," *AIP Conference Proceedings*, Vol:1851, 020006. http://dx.doi.org/10.1063/1.4984635

Arifuzzaman, S. M., Khan, M. S., Islam., B. M. J. Rana, P. Biswas and Ahmmed, 2017b, "MHD Maxwell fluid flow in presence of nano-particle through a vertical 2 porous–plate with heat- generation, radiation absorption and chemical reaction," *Frontiers in Heat and Mass Transfer*,**9** (25), 1-14. http://dx.doi.org/10.5098/hmt.9.25.

Arifuzzaman,S.M., Khan, M.S., Hossain., Islam., Akter and R. Roy, 2017c, "Chemically reactive viscoelastic fluid flow in presence of nano

particle through porous stretching sheet," *Frontiers in Heat and Mass Transfer*,**9**(5),111.
http://dx.doi.org/10.5098/hmt.9.5

Biswas, P., Arifuzzaman, S.M., Karim, I. and Khan, M.S., 2017, "Impacts of Magnetic Field and Radiation Absorption on Mixed Convective Jeffrey Nano Fluid Flow over a Vertical Stretching Sheet with Stability and Convergence Analysis," *Journal of nanofluids*, **6**(6), 1082-1095.
https://doi.org/10.1166/jon.2017.1407

Bujurke, N. M., Pai, N. P. and Jayaraman, G., 1998, "Computer extended series solution for unsteady flow in a contracting or expanding pipe," *IMA Journal of Applied Mathematics*, **60**,151–165.

Dauenhauer, E. C. and Majdalani, J., 1999, "Unsteady flows in semi-infinite expanding channels with wall injection", *AIAA paper*, 99–3523.
https://doi.org/10.2514/6.1999-3523

Eldabe, N. T. M., Salwa, M. G. E., 1995, "Heat transfer of MHD non-Newtonian Casson fluid flow between two rotating cylinders," *J. Phys. Soc*. Japan, 64, 41.

Fung, Y.C., Yih, C.S., 1968, Peristaltic transport. *Journal of Applied Mechanics,* **35**, 669–675.

Goto, M. and Uchida, S., 1980, "Unsteady flow in a semi-infinite expanding pipe with injection through wall", *Journal of the Japan Society for Aeronautical and Space Science*, **38** (434), 131–138.

Hari R.Kataria, Harshad R Patel., 2016, "The Soret and heat generatio effects on MHD Casson flid past an oscillating vertical plate embedded through porous medium."55(3), 1903-3036.
https://doi.org/10.1016/j.aej.2016.06.024

Hayat, T. Shehzad, S. A. Qasim, M. and Obaidat, S., 2012, "Radiative flow of Jeffrey fluid in a pus medium with power law heat flux and heat source," *Nuclear Engineering and Design*, 243, 15–19.

Hossain, M.A., Khanafer, K. and Vafai, K., 2001, "The effect of radiation on free convection flow of fluid with variable viscosity from a porous vertical plate," *Int. J. Therm. Sci.*, **40**, 115–124.
https://doi.org/10.1016/S1290-0729(00)01200-X

Khan,M.S., Karim, Ali, L. E. , and Islam, 2012, "Unsteady MHD free convection boundary-layer flow of a nanofluid along a stretching sheet with thermal radiation and viscous dissipation effects," *International Nano Letters*, **2**, 24.

Majdalani, J., Zhou, C., and Dawson, C.A., 2002, "Two-dimensional viscous flows between slowly expanding or contracting walls with weak permeability," *Journal of Biomechanics*, **35**, pp. 1399–1403.
https://doi.org/10.1016/S0021-9290(02)00186-0

Majdalani, J. and Zhou, C., 2003, "Moderate-to-large injection and suction driven channel flows with expanding and contracting walls", *ZAMM. Zeitschrift fur Angewandte Mathematik und Mechanik*, **83**, 181–196.
http://DOI 10.1002/zamm.200310018

Makinde, OD., Mutuku.W.N., 2014, "Hydromagnetic thermal boundary layer of nanofluids over a convectively heated flat plate with viscous dissipation and Ohmic heating," *U.P.B. Sci. Bull. Ser. A*, **76**(2):181–92.

Odelu Ojjela and Naresh kumar., 2016, "Chemically reacting micropolar fluid flow and heat transfer between expanding or contracting walls with ion slip, Soret and Dufour effects," *Alexandria Engineering Journal*, **55(2)**, 1683-1694.
https://doi.org/10.1016/j.aej.2016.02.026

Ohki, M., 1980, "Unsteady flows in a porous, circular tube–1 the wall contracting or expanding in an axial direction", *Bulletin of the JSME*, 23,679–686.
https://doi.org/10.1299/jsme1958.23.679

Olarewaju. P.O., 2012, "Similarity solution for natural convection from a moving vertical plate with internal heat generation and a convective boundary condition in the presence of thermal radiation and viscous dissipation," *J Rep Opin* , **4**(8), 68–76.

Partha, M. K., 2009, "Suction/injection effects on thermophoresis particle deposition in a non-Darcy porous medium under the influence of Soret, Dufour effects," *Int. J. Heat and Mass Transfer*, **52**, 1971–1979.
https://doi.org/10.1016/j.ijheatmasstransfer.2008.07.055

Sarojamma, G., Ramana, B. and Vendabai, K., 2014, "Heat and mass transfer on MHD boundary layer flow of a chemically reacting non-Newtonian fluid over a stretching sheet with suction," *Int. J. Engineering Sciences & Research Technology*, **3**(5), 197–205.

Seth, G. S., Ansari, Md. S., Nandkeolyar, R., 2010, "MHD Natural Convection Flow past an Impulsively Moving Vertical Plate with Ramped wall Temperature in the Presence of Thermal Diffusion with Heat absorption," *International Journal of Applied Mechanics and Engineering*, **15**, 199–215.
https://doi.org/10.1007/s00231-010-0740-1

Singh, A. K., 2008, "Heat source and radiation effect on magneto-convection flow of a viscoelastic fluid past a stretching sheet: Analysis with Kummer's function", *Int. J. Commun. in Heat Mass Transfer*, **35**, 637–642.
DOI: 10.1016/j.icheatmasstransfer.2008.01.009

Subhakar MJ, Gangadhar, 2012, "Soret and Dufour effects on MHD free convection heat and mass transfer flow over a stretching vertical plate with suction and heat source/sink," *Int J Mod Eng Res*, :3458–68.

Uchida, S. and Aoki, H., 1977, "Unsteady flows in a semi-infinite contracting or expanding pipe," *Journal of Fluid Mechanics*, **82**, 371–387.
https://doi.org/10.1017/S0022112077000718

Vempati, S. R. and Laxmi-Narayana-Gari, A. B., 2010, "Soret and Dufour effects on unsteady MHD flow past an infinite vertical porous plate with thermal radiation," *Appl. Math. Mech. Engl. Ed*, **31**(12), 1481–1496.

Vijaya,N., sreelakshmi., Sarojamma,G., 2017, "Non-linear radiation effect on Casson fluid Saturated Non Darcy porous medium," *International Journal of Mathematical Archive*-**8**(2), 39-52.

Vijayalakshmi, R., Sarojamma,G., Sreelakshmi,K. Sandhya.G., 2017, "Unsteady flow of a cassion fluid through a vertical channel with walls of expansion and contraction," *International Journal of Research In Science & Engineering,* Special Issue –NCRAPAM, 186-197.

Womersley, J.R., 1955, "Method for the calculation of velocity, rate of flow and viscous drag in arteries when the pressure gradient is known," *Journal of Physiology*, **127**, 553–563.